

Effective use of Spatial and Spectral Correlations for Color Filter Array Demosaicking

Lanlan Chang and Yap-Peng Tan, Member, IEEE

Abstract — *To minimize cost and size, most commercial digital cameras acquire imagery using a single electronic sensor (CCD or CMOS) overlaid with a color filter array (CFA) such that each sensor pixel only samples one of the three primary color values. To restore a full-color image from CFA samples, the two missing color values at each pixel need to be estimated from the neighboring samples, a process that is commonly known as CFA demosaicking or interpolation. In this paper we present two contributions to CFA demosaicking. First, we stress the importance of well exploiting both image spatial and spectral correlations, and characterize the demosaicking artifacts due to inadequate use of either correlation. Second, based on the insights gained from our empirical study, we propose effective schemes to enhance two existing state-of-the-art demosaicking methods. Experimental results show that our enhanced methods achieve notable improvements over the existing methods, in terms of both subjective and objective evaluations, on a large variety of test images. In addition, the computational complexities of the enhanced methods are comparable to the originals.*¹

Index Terms — Digital camera, color filter array, demosaicking, spatial correlation, spectral correlation.

I. INTRODUCTION

Digital still cameras (DSCs) have gained strong favor with consumers and replaced their film-based counterparts in many applications over the past few years. To reduce their cost and size for increased manufacturability and competitiveness, most DSCs acquire imagery using a single electronic sensor (CCD or CMOS) overlaid with a color filter array (CFA). The CFA consists of a mosaic of colored filters such that each sensor pixel measures only one of the three primary colors (e.g., red, green, and blue). The most commonly used CFA pattern is probably the Bayer CFA pattern [1], a schematic diagram of which is shown in Fig. 1(a). In this pattern, red and blue values are sampled on rectangular lattices, while green values are measured on a quincunx lattice, twice as many as that of the red or blue values. The rationale behind having a denser green samples in this CFA pattern is that the green filter has a spectral response close to the luminance response of human visual system, recording most spatial information consequential to perceived image quality [3].

To reconstruct a full-color image from CFA samples, the two missing color values at each pixel are to be estimated from neighboring CFA samples. This process is commonly known as CFA demosaicking or interpolation, and a large number of

demosaicking methods have been proposed in the literature [2-15]. Among them, the simplest and most referenced is probably bilinear interpolation [2,3], which fills in a missing color value with the average of its neighboring CFA samples of the same color—four samples for each missing green value and two for a missing red or blue value in the Bayer CFA pattern (see Fig. 1(a)). However, because this simple interpolation method does not consider the presence of object boundaries and indiscriminately combines color values across edges, it often blurs fine image details and produces highly visible artifacts around image edge regions.

To restore more accurate and visually pleasing results, many sophisticated demosaicking methods have been proposed exploiting image spatial or spectral correlation, or both. Image spatial correlation refers to the fact that within a homogeneous image region, neighboring pixels share similar color values, while spectral correlation dictates that there is a high correlation between the red, green and blue image planes, resulting in that the difference (or ratio) between two color planes is likely to be a constant within a local image neighborhood. Exploiting spatial correlation, for example, Zen *et al.* propose to fill in the missing color values by replicating their nearest neighboring values [4]; Adams proposes to estimate the missing color values according to different local color intensity patterns [5]; and the edge-sensing methods [5,6] interpolate along the edge direction determined by a number of edge indicators. As for the spectral correlation, Cok [7] proposes a constant hue method to estimate the missing red and blue values by using the color ratios (red/green and blue/green) within a local image neighborhood. Because the ratio of two color values in linear exposure space is approximately equal to their difference in logarithmic (or gamma-corrected) exposure space, a few other methods, including the gradient-based interpolation [8], new edge-directed interpolation [9], and the recent effective color interpolation [10] advocate to interpolate the color difference values (green minus red and green minus blue) for the missing red and blue values.

Unlike the above-mentioned methods using either spatial or spectral correlation, some recent methods manage to exploit both correlations. Representative methods include Freeman's method [11] using a median filter to process color difference values for removing artifacts around edges, Hamilton and Adams's method [12] performing edge-adaptive interpolation in color difference planes, Kimmel's method and Hur and Kang's method [13,14] combining the use of smooth hue transition and edge-adaptive interpolation schemes, and Gunturk *et al.*'s method [15] making use of an edge-adaptive scheme and alternating the high frequency subbands of green and red/blue planes to estimate the missing color values. Experimental comparisons [2,15] have demonstrated that these methods, exploiting both correlations, can achieve superior

¹ The authors are with the School of Electrical & Electronic Engineering, Nanyang Technological University, Singapore (e-mail: CHAN0069@ntu.edu.sg; eyptan@ntu.edu.sg).

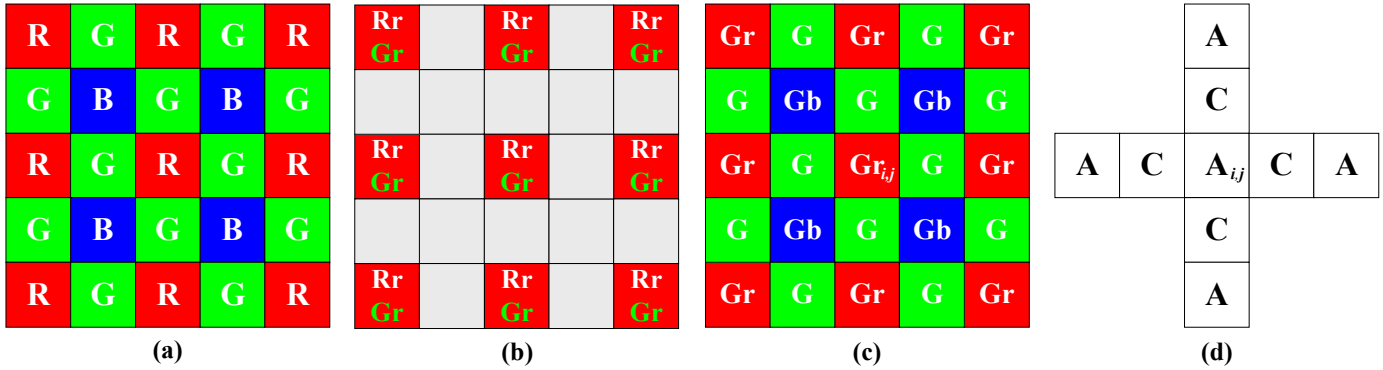


Fig. 1. (a) Bayer color filter array; (b) Down-sampled red samples (Rr, measured) and green samples (Gr, interpolated); (c) Reference neighboring samples for the enhanced AP method; (d) Reference neighboring samples for the enhanced ECI method (A and C denote red, green, or blue values); subscripts i and j are row and column indexes, respectively.

objective and subjective qualities than those using only either spatial or spectral correlation. However, as we will show in this paper, many of these methods have not made full and effective use of both correlations, and hence can only obtain sub-optimal demosaicking results.

Particularly, by comparing the results obtained from various existing demosaicking methods, we have observed that those methods that do not well exploit spatial correlation often produce zipper-effect artifacts—artificial “on-off” patterns created in smooth regions around edges and mainly caused by improper fusion of neighboring color values cross edge—as shown in Fig. 2(a). On the other hand, those that inaccurately utilize the spectral correlation often result in false color artifacts—noticeable color errors or fringes around fine image details and edges—as seen in Fig. 2(b). These two types of artifacts severely degrade the perceived quality of the demosaicked images.

produce highly visible zipper-effect artifacts around sharp edges because of inadequate use of spatial correlation. Sample results obtained by these two methods are shown in Fig. 3. By effectively exploiting the spatial correlation, our enhanced methods obtain notable improvements over the original methods, in terms of both visual comparison and peak-signal-to-noise-ratio (PSNR) evaluation, on a large variety of test images.

The remainder of the paper is organized as follows. Section II reviews the original algorithms of the two existing state-of-the-art methods to be enhanced. Section III describes our schemes to enhance these two existing methods. The experimental results and complexity analysis of the methods under comparison are presented in Section IV and Section V, respectively. The conclusion of the paper is given in Section VI.

II. TWO EXISTING DEMOSAICKING METHODS

In this section, we briefly review the two state-of-the-art methods that we improved: effective color interpolation (ECI) method [10] and alternating-projections (AP) method [15].

A. ECI method

The ECI method exploits mainly the image spectral correlation by performing bilinear interpolation on two color difference planes: $K_R \equiv G - R$ and $K_B \equiv G - B$. The method works as follows:

- 1). **Green plane interpolation:** Each missing green value is first estimated by using the average of its neighboring color difference values. As shown in Fig. 4(a), to obtain the missing $G_{i,j}$ (green) value at the $R_{i,j}$ (red) pixel, the method first computes the K_R color difference values at the four surrounding locations: $(i-1, j)$, $(i+1, j)$, $(i, j-1)$, and $(i, j+1)$. Since there are only G but no R values at these locations, the K_R values are obtained by estimating the R values from the two adjacent R samples as follows:



Fig. 2. Two common demosaicking artifacts. (a) Zipper-effect artifacts. (b) False color artifacts.

We therefore argue in this paper that only when both spatial and spectral correlations are well exploited, these artifacts can be effectively suppressed to restore high-quality color images. We support this point by enhancing the performance of two existing state-of-the-art demosaicking methods—effective color interpolation method [10] and alternating-projections method [15]—through effective use of both correlations. Specifically, although these two existing methods have been reported to be capable of achieving superior demosaicking results as compared with other existing methods [10,15], they

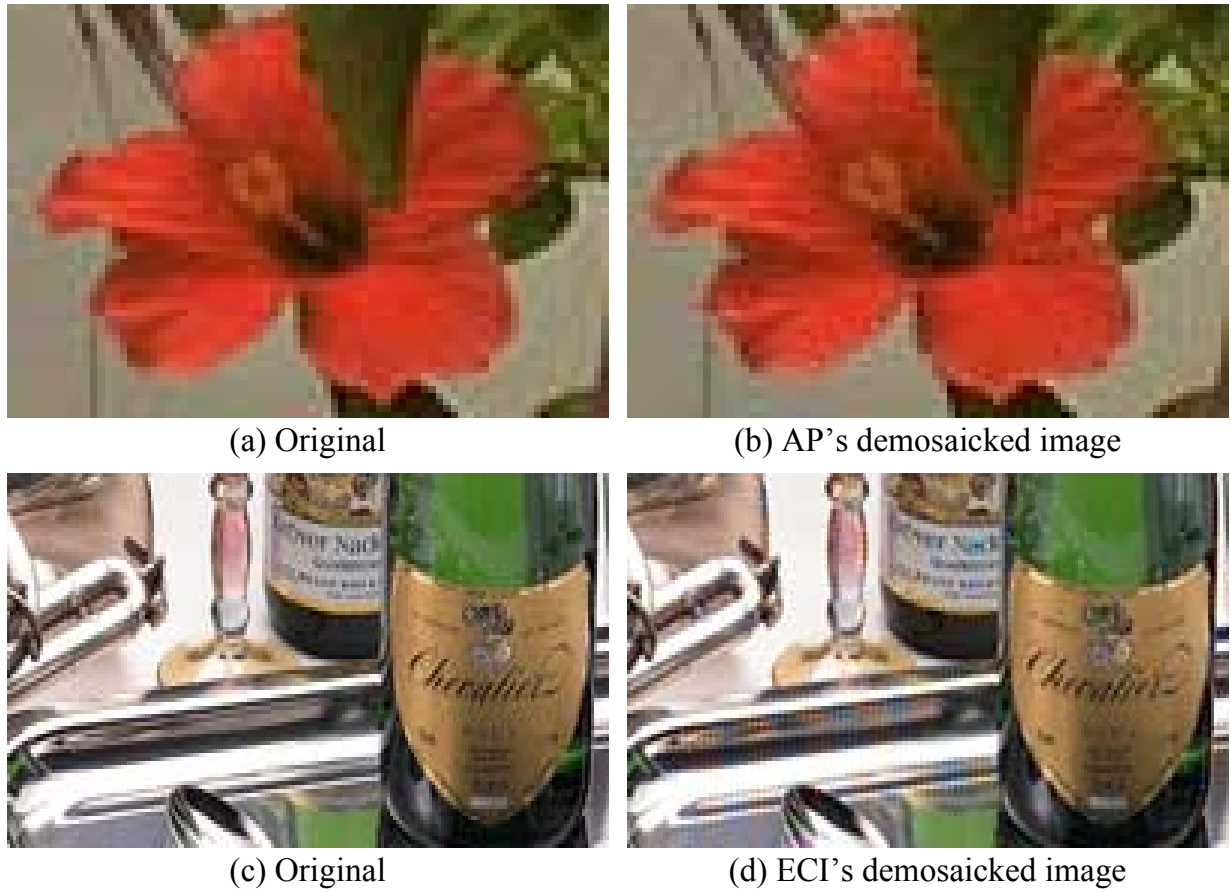


Fig. 3. Zipper-effect artifacts in the demosaicked images obtained by the original AP and ECI methods.

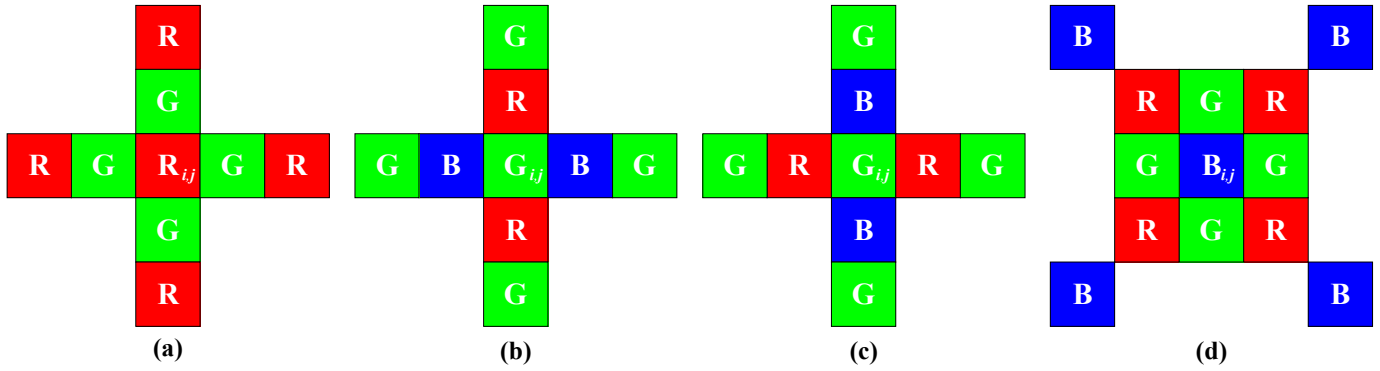


Fig. 4. Reference CFA samples, where subscripts i and j represent row and column indexes, respectively.

$$\begin{aligned}
 \tilde{K}_{R(i-1,j)} &= G_{i-1,j} - \tilde{R}_{i-1,j} = G_{i-1,j} - \frac{1}{2}(R_{i-2,j} + R_{i,j}) \\
 \tilde{K}_{R(i+1,j)} &= G_{i+1,j} - \tilde{R}_{i+1,j} = G_{i+1,j} - \frac{1}{2}(R_{i+2,j} + R_{i,j}) \\
 \tilde{K}_{R(i,j-1)} &= G_{i,j-1} - \tilde{R}_{i,j-1} = G_{i,j-1} - \frac{1}{2}(R_{i,j-2} + R_{i,j}) \\
 \tilde{K}_{R(i,j+1)} &= G_{i,j+1} - \tilde{R}_{i,j+1} = G_{i,j+1} - \frac{1}{2}(R_{i,j+2} + R_{i,j}).
 \end{aligned} \tag{1}$$

The missing green value is then obtained as

$$\tilde{G}_{i,j} = R_{i,j} + \frac{1}{4}(\tilde{K}_{R(i-1,j)} + \tilde{K}_{R(i+1,j)} + \tilde{K}_{R(i,j-1)} + \tilde{K}_{R(i,j+1)}) \tag{2}$$

Note that in our notation, \tilde{x} denotes an estimated value, while x represents the value obtained from the original CFA sample(s), where x can be R , G , B , K_R , or K_B value.

The missing G values at B (blue) pixels can be similarly estimated using the K_B color difference values.

2). **Red/Blue plane interpolation:** Once the green plane has been fully populated, it is used to compute the neighboring K_R and K_B values for estimating the missing R and B values. Referring to Fig. 4(b), the missing $R_{i,j}$ value at the $G_{i,j}$ pixel is estimated as

$$\tilde{R}_{i,j} = G_{i,j} - \frac{1}{2}(\tilde{K}_{R(i-1,j)} + \tilde{K}_{R(i+1,j)}). \quad (3)$$

Similarly, the missing $R_{i,j}$ value at the $G_{i,j}$ pixel shown in Fig. 4(c) is calculated as

$$\tilde{R}_{i,j} = G_{i,j} - \frac{1}{2}(\tilde{K}_{R(i,j-1)} + \tilde{K}_{R(i,j+1)}) \quad (4)$$

Then, the missing $R_{i,j}$ value at the $B_{i,j}$ pixel shown in Fig. 4(d) is obtained as

$$\tilde{R}_{i,j} = \tilde{G}_{i,j} - \frac{1}{4}(\tilde{K}_{R(i-1,j)} + \tilde{K}_{R(i+1,j)} + \tilde{K}_{R(i,j-1)} + \tilde{K}_{R(i,j+1)}) \quad (5)$$

The missing B values can be similarly estimated with the use of the K_B values.

B. AP method

The AP method exploits the high spectral correlation between different color planes for estimating the missing color values by alternately projecting their estimates onto two constraint sets. The first constraint set imposes consistency between the original CFA samples and the corresponding color values in the demosaicked color planes. The second constraint set, an exploitation of the high image spectral correlation, enforces the similarity between the high-frequency subbands of two color planes. To meet the second constraint set, each color plane is decomposed using a low-pass and a high-pass analysis filters into four subbands: 1) LL: an approximation subband whose rows and columns are low-pass filtered; 2) LH: a vertical subband whose rows are low-pass filtered and columns are high-pass filtered; 3) HL: a horizontal subband whose rows are high-pass filtered and columns are low-pass filtered; and 4) HH: a diagonal subband whose rows and columns are high-pass filtered.

The method works as follows:

1). **Initial interpolation:** This step uses an edge-adaptive demosaicking method [12] to interpolate the green plane and bilinear interpolation to populate the red and blue planes. Specifically, with reference to Fig. 4(a), the missing $G_{i,j}$ value at the $R_{i,j}$ pixel is estimated as follows. First, two values are computed to determine the dominant edge direction:

$$\begin{aligned} DH &= |-R_{i,j-2} + 2R_{i,j} - R_{i,j+2}| + |G_{i,j-1} - G_{i,j+1}| \\ DV &= |-R_{i-2,j} + 2R_{i,j} - R_{i+2,j}| + |G_{i-1,j} - G_{i+1,j}|. \end{aligned} \quad (6)$$

Then, the green value $G_{i,j}$ is estimated along the dominant edge direction by Eq. (7).

The estimation for the missing G value at a B pixel is processed similarly.

$$\tilde{G}_{i,j} = \begin{cases} \frac{G_{i,j-1} + G_{i,j+1}}{2} + \frac{-R_{i,j-2} + 2R_{i,j} - R_{i,j+2}}{2} & \text{if } DH < DV \\ \frac{G_{i-1,j} + G_{i+1,j}}{2} + \frac{-R_{i-2,j} + 2R_{i,j} - R_{i+2,j}}{2} & \text{if } DH > DV \\ \frac{G_{i-1,j} + G_{i,j-1} + G_{i,j+1} + G_{i+1,j}}{4} + \frac{-R_{i-2,j} - R_{i,j-2} + 4R_{i,j} - R_{i,j+2} - R_{i+2,j}}{8} & \text{if } DH = DV \end{cases} \quad (7)$$

$$\begin{aligned} Gr(n_1, n_2) &= \text{Rec}(Gr_{LL}(n_1, n_2), Rr_{LH}(n_1, n_2), Rr_{HL}(n_1, n_2), Rr_{HH}(n_1, n_2)) \\ &\equiv g_0(n_1) * [g_0(n_2) * Gr_{LL}(n_1, n_2)] + g_0(n_1) * [g_1(n_2) * Rr_{LH}(n_1, n_2)] \\ &\quad + g_1(n_1) * [g_0(n_2) * Rr_{HL}(n_1, n_2)] + g_1(n_1) * [g_1(n_2) * Rr_{HH}(n_1, n_2)] \end{aligned} \quad (9)$$

Next, the red plane is populated by bilinear interpolation as follows:

(a). For the $R_{i,j}$ value at the $G_{i,j}$ pixel as shown in Fig. 4(b):

$$\tilde{R}_{i,j} = \frac{1}{2}(R_{i-1,j} + R_{i+1,j})$$

(b). For the $R_{i,j}$ value at the $G_{i,j}$ pixel as shown in Fig. 4(c):

$$\tilde{R}_{i,j} = \frac{1}{2}(R_{i,j-1} + R_{i,j+1})$$

(c). For the $R_{i,j}$ value at the $B_{i,j}$ pixel as shown in Fig. 4(d):

$$\tilde{R}_{i,j} = \frac{1}{4}(R_{i-1,j-1} + R_{i+1,j+1} + R_{i+1,j-1} + R_{i-1,j+1})$$

Then, the blue plane is similarly populated as the red plane.

2). Green plane updating:

(a) The measured red CFA samples are aggregated to form a down-sampled red plane (Rr), and the interpolated green values at the locations of these red samples are merged to form the corresponding down-sampled green plane (Gr), as shown in Fig. 1(b).

(b) Decompose the two down-sampled planes into four subbands (LL, LH, HL, and HH), given by

$$\begin{aligned} S_{LL}(n_1, n_2) &= h_0(n_1) * [h_0(n_2) * S(n_1, n_2)] \\ S_{LH}(n_1, n_2) &= h_0(n_1) * [h_1(n_2) * S(n_1, n_2)] \\ S_{HL}(n_1, n_2) &= h_1(n_1) * [h_0(n_2) * S(n_1, n_2)] \\ S_{HH}(n_1, n_2) &= h_1(n_1) * [h_1(n_2) * S(n_1, n_2)], \end{aligned} \quad (8)$$

where (n_1, n_2) denotes the pixel coordinates, $h_0 = [1 \ 2 \ 1]/4$ and $h_1 = [1 \ -2 \ 1]/4$ are the low-pass and high-pass analysis filters, respectively, and S designates the two down-sampled color planes, Rr and Gr .

(c) Replace the high-frequency subbands (LH, HL, and HH) of the Gr plane with that of the Rr plane, and then reconstruct the Gr plane by using Eq. (9), where $g_0 = [-1 \ 2 \ 6 \ 2 \ -1]/8$ and $g_1 = [1 \ 2 \ -6 \ 2 \ 1]/8$ are the low-pass and high-pass synthesis filters, respectively.

(d) Insert the reconstructed green values into their corresponding locations in the full-size green plane obtained from the initial interpolation step.

The updating of the estimated green values at blue pixels (i.e., the Gb plane) is similarly performed using the down-sampled blue plane (Bb).

3). **Detail projection:** Decompose each of the three estimated full-color planes— \tilde{R} , \tilde{G} , and \tilde{B} —into four subbands, and replace the high-frequency subbands (LH, HL, and HH) of the \tilde{R} and \tilde{B} planes with that of the \tilde{G} plane to refine the \tilde{R} and \tilde{B} planes as

$$\begin{aligned}\tilde{R} &= \text{Rec}(\tilde{R}_{LL}, \tilde{G}_{LH}, \tilde{G}_{HL}, \tilde{G}_{HH}) \\ \tilde{B} &= \text{Rec}(\tilde{B}_{LL}, \tilde{G}_{LH}, \tilde{G}_{HL}, \tilde{G}_{HH}).\end{aligned}\quad (10)$$

4). **Observation projection:** For those color samples which are originally available in the CFA pattern, replace them from the reconstructed \tilde{R} , \tilde{G} and \tilde{B} planes with their original CFA samples to preserve the “observed” or “measured” values.

5). **Iteration:** Repeat the detail projection step and the observation projection step for a preset number of times (typically 3-5 times).

III. PROPOSED ENHANCED METHODS

In this section, we present the proposed enhanced ECI and AP methods. The block diagrams of the enhanced methods are shown in Fig. 5.

A. Enhanced ECI method

Although the original ECI method can obtain reasonably good demosaicking image quality with a low computational cost, it takes no account of the fact that the color difference planes are not as uniform as assumed. Consequently, applying bilinear interpolation indiscriminately on the color difference planes would over smooth them, resulting in zipper-effect artifacts around image edge regions, as illustrated in Fig. 3(d). To suppress such highly visible artifacts, we propose an adaptive weighted interpolation scheme in the enhanced ECI method for preserving the details in the color difference planes.

Before elucidating the algorithm of the enhanced ECI method, we first show how to obtain the weighted color difference values around a pixel under consideration. Refer to Fig. 1(d), where A and C denote R , G , or B values. Generally, A designates a value from the original CFA samples, while some C values could be estimates from their neighboring values; for example, when A is a green value (see Fig. 4(b) and Fig. 4(c)), two of the adjacent R (or B) values are from the original CFA samples and the other two R (or B) values are estimated values. To obtain the color difference value K_X at pixel (i, j) under consideration, where K_X could be either K_R or K_B depending on the colors of A and C , we first calculate the weights along the four adjacent directions as follows:

$$\begin{aligned}\alpha_{i-1,j} &= |A_{i-2,j} - A_{i,j}| + |C_{i-1,j} - C_{i+1,j}| \\ \alpha_{i+1,j} &= |A_{i+2,j} - A_{i,j}| + |C_{i+1,j} - C_{i-1,j}| \\ \alpha_{i,j-1} &= |A_{i,j-2} - A_{i,j}| + |C_{i,j-1} - C_{i,j+1}| \\ \alpha_{i,j+1} &= |A_{i,j+2} - A_{i,j}| + |C_{i,j+1} - C_{i,j-1}|.\end{aligned}\quad (11)$$

The weights are then assigned to the four adjacent color difference values \tilde{K}_X , as defined in (1), for estimating $K_{X(i,j)}$ as

$$\tilde{K}_{X(i,j)} = \frac{\frac{\tilde{K}_{X(i-1,j)}}{1+\alpha_{i-1,j}} + \frac{\tilde{K}_{X(i+1,j)}}{1+\alpha_{i+1,j}} + \frac{\tilde{K}_{X(i,j-1)}}{1+\alpha_{i,j-1}} + \frac{\tilde{K}_{X(i,j+1)}}{1+\alpha_{i,j+1}}}{\frac{1}{1+\alpha_{i-1,j}} + \frac{1}{1+\alpha_{i+1,j}} + \frac{1}{1+\alpha_{i,j-1}} + \frac{1}{1+\alpha_{i,j+1}}}.\quad (12)$$

Referring to the block diagram in Fig. 5, we now describe the two successive steps of the proposed enhanced ECI method: initial step and refinement step.

1). **Initial step:** In this step, the missing green values at red and blue pixels are first estimated. Referring to Fig. 4(a) as an example, the color difference value $\tilde{K}_{R(i,j)}$ is computed with (12) by setting K_X to K_R and using the four adjacent \tilde{K}_R values obtained by (1); the associated weights are computed by (11) with A set to R and C set to G . The missing green value at the red pixel is then computed as

$$\tilde{G}_{i,j} = R_{i,j} + \tilde{K}_{R(i,j)}\quad (13)$$

The missing G values at B pixels can be similarly estimated using the adjacent \tilde{K}_B values.

Next, the red and blue planes are interpolated with the aid of the populated green plane. The missing red values at blue pixels are estimated with a similar adaptive weighted scheme using the four adjacent \tilde{K}_R values— $\tilde{K}_{R(i-1,j-1)}$, $\tilde{K}_{R(i+1,j+1)}$, $\tilde{K}_{R(i+1,j-1)}$, and $\tilde{K}_{R(i-1,j+1)}$ —as shown in Fig. 4(d). The weights along the four adjacent directions are obtained as

$$\begin{aligned}\alpha_{i-1,j-1} &= |B_{i-2,j-2} - B_{i,j}| + |R_{i-1,j-1} - R_{i+1,j+1}| \\ \alpha_{i+1,j+1} &= |B_{i+2,j+2} - B_{i,j}| + |R_{i+1,j+1} - R_{i-1,j-1}| \\ \alpha_{i+1,j-1} &= |B_{i+2,j-2} - B_{i,j}| + |R_{i+1,j-1} - R_{i-1,j+1}| \\ \alpha_{i-1,j+1} &= |B_{i-2,j+2} - B_{i,j}| + |R_{i-1,j+1} - R_{i+1,j-1}|.\end{aligned}\quad (14)$$

The $K_{R(i,j)}$ value is then estimated by

$$\tilde{K}_{R(i,j)} = \frac{\frac{\tilde{K}_{R(i-1,j-1)}}{1+\alpha_{i-1,j-1}} + \frac{\tilde{K}_{R(i+1,j+1)}}{1+\alpha_{i+1,j+1}} + \frac{\tilde{K}_{R(i+1,j-1)}}{1+\alpha_{i+1,j-1}} + \frac{\tilde{K}_{R(i-1,j+1)}}{1+\alpha_{i-1,j+1}}}{\frac{1}{1+\alpha_{i-1,j-1}} + \frac{1}{1+\alpha_{i+1,j+1}} + \frac{1}{1+\alpha_{i+1,j-1}} + \frac{1}{1+\alpha_{i-1,j+1}}}\quad (15)$$

with K_X set to K_R . The missing $R_{i,j}$ value is then obtained as

$$\tilde{R}_{i,j} = \tilde{G}_{i,j} - \tilde{K}_{R(i,j)}.\quad (16)$$

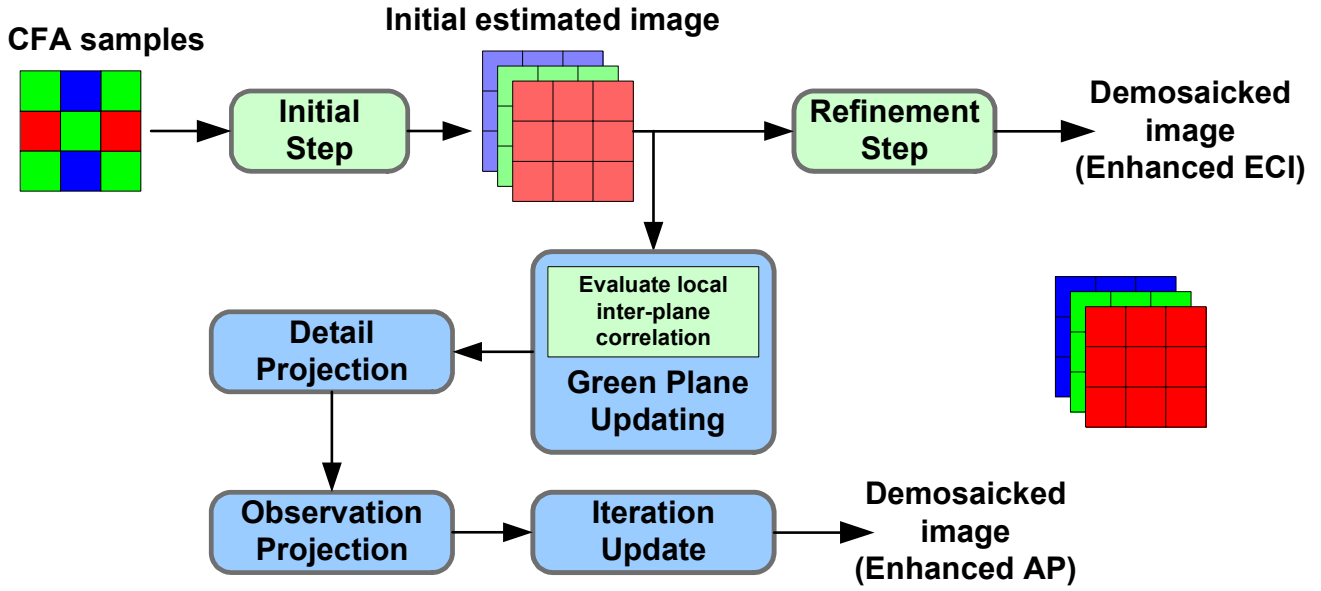


Fig.5. Block diagrams of the proposed enhanced ECI and AP methods.

Once all the missing red values at blue pixels have been obtained, the four adjacent \tilde{K}_R values around the missing red values at green pixels become readily available. We then compute the weights of these adjacent color difference values by using (1) (with A as G and C as R) and estimate the missing red values (see Fig. 4(b) and Fig. 4(c)) by using (12) (with K_X as K_R) and (16) to fully populate the red plane.

The missing blues values can be similarly estimated using the adjacent \tilde{K}_B values.

2). **Refinement step:** In the initial step, the estimation for the missing green values and that for the missing red and blue values are processed differently due to their sampling difference in the CFA pattern. After the initial step, the three color planes are fully populated, and their estimates can be further refined by using the same interpolation scheme to generate more consistent color values and thus reduce demosaicking artifacts. This is accomplished by assigning weights calculated with (11) to their four adjacent color difference values obtained from the initial step, and the refining the estimates by using (12) as well as (13) or (16).

B. Enhanced AP method

The enhancement we make to the original AP method mainly lies in the initial interpolation step and green plane updating step. First, we replace the initial interpolation step with that of the enhanced ECI method as described in Section III-A; this is to improve the accuracy of the initial estimates of the three color planes by more effectively exploiting the spatial correlation. Second, we modify the green plane updating step to make it adaptive to local spectral correlation. The original AP method works under the premise of high correlation between the high-frequency subbands of the green and

blue/red planes [15]. Specifically, because the red, green, and blue CFA samples are measured at different pixel locations, the high-frequency subbands of the red/blue plane samples can be used to replace the corresponding subbands of the interpolated green values for refining the estimates. However, such high spectral correlation is evident only when considering the entire color planes as a whole [15]; the local correlations between two color planes may not be as high at all pixel locations. Consequently, replacing the high-frequency subbands between two different color planes indiscriminately may produce errors around sharp edges, where the inter-plane correlation is usually not high. For an example, see the zipper-effect artifacts shown in Fig. 3(b).

With this in mind, our enhanced AP method exploits the intra-plane spatial correlation instead of inter-plane spectral correlation in edge regions, where the high-frequency subbands of different color planes are not highly correlated. More precisely, we make use of the fact that the values along the rows of the LH subband are highly correlated because the rows are low-pass filtered and the columns are high-pass filtered. Similarly, high correlation holds for the values along the columns of the HL subband. Hence, when the local spectral correlation is not high, the LH and HL subbands of the observed green plane can be interpolated along the row and column, respectively, and be used as the corresponding subbands for estimating the missing green values at the red and blue pixels.

Specifically, to update the green plane, we compute the local inter-plane correlation using the initial estimates of two color planes as given by Eq. (17),

$$Corr_{local}(r,s) = \frac{\sum_{m=r-w/2}^{r+w/2} \sum_{n=s-h/2}^{s+h/2} (x(m,n) - \mu_x)(y(m,n) - \mu_y)}{\sqrt{\sum_{m=r-w/2}^{r+w/2} \sum_{n=s-h/2}^{s+h/2} (x(m,n) - \mu_x)^2} \sqrt{\sum_{m=r-w/2}^{r+w/2} \sum_{n=s-h/2}^{s+h/2} (y(m,n) - \mu_y)^2}} \quad (17)$$

where (r, s) represents the pixel coordinates, x denotes the red or blue value, y denotes the green value, and μ_x and μ_y are the average of x and y values in a local window consisting of $(w+1) \times (h+1)$ pixels. If the local inter-plane correlation around pixel (r, s) is larger than some predetermined threshold T_c , the green value estimated from the original AP method is used; otherwise, it is obtained from an alternative green plane whose high-frequency subbands are obtained by interpolating that of the observed green plane along the direction of low-pass filtering. In our experiments, the size of the local window is set to 5×5 (i.e., w and h are equal to 4) and threshold T_c is set to 0.95.

Referring to Fig. 1(c) as an example, the missing green values at the red pixels are interpolated as follows:

- Obtain the interpolated LH and HL subbands as

$$\begin{aligned}\tilde{G}r_{LH} &= f_0(n1) * Gg_{LH} \\ \tilde{G}r_{HL} &= f_0(n2) * Gg_{HL},\end{aligned}\quad (18)$$

where $f_0 = [1 \ 3 \ 3 \ 1]/8$.

- Reconstruct the alternative green plane $\tilde{G}r$ by using the interpolated $\tilde{G}r_{LH}$ and $\tilde{G}r_{HL}$ subbands as:

$$\tilde{G}r = \text{Rec}(Gg_{LL}, \tilde{G}r_{LH}, \tilde{G}r_{HL}, Rr_{HH}). \quad (19)$$

The missing green values at blue pixels (i.e., the $\tilde{G}b$ plane) can be updated similarly.

IV. EXPERIMENTAL RESULTS

To evaluate the performance of our proposed enhanced methods, we compare their demosaicked results with those of the five existing demosaicking methods—bilinear interpolation, median filter method (Freeman) [11], new edge directed interpolation (NEDI) [9], original ECI method [10], and original AP method [15]. Among the methods under comparison, bilinear interpolation is the simplest and also the most common reference benchmark for comparison in CFA demosaicking literature. Both Freeman's method and NEDI method can obtain good demosaicking results as reported in [2,9,11]. The original ECI and AP methods, which we improved, are the recent state-of-the-art methods that can produce superior results as presented in [10,15] and confirmed by our empirical study.

Fig. 6 shows our test image set, of which many have been used in CFA demosaicking research and experiments [2,9,10,13,15]. In what follows, we evaluate the performance of the proposed enhanced methods from two aspects: subjective visual comparison and objective PSNR comparison.

A. Visual comparison

Figs. 7, 8, and 9 show the cropped regions from three original test images (Images 3, 9 and 27 in Fig. 6) and the corresponding regions reconstructed by the original and our enhanced ECI and AP methods. Observably, the demosaicked results obtained by our enhanced methods incur much fewer zipper-effect artifacts, as compared with that of the original

ECI and AP methods, e.g., along the boundary of the cap in Fig. 7, the border between two colors on the sail in Fig. 8, and the circumferences of the fruits in Fig. 9.

B. PSNR comparison

The PSNR performances of the methods under comparison are listed in Table I. The table shows that our enhanced methods outperform others in terms of PSNR results with almost all test images. In particular, the average PSNR improvements of the enhanced ECI method over the original ECI method in red, green, and blue planes are 2.33 dB, 3.41 dB and 2.49 dB, respectively, while those of the enhanced AP method over the original AP method are 0.65 dB, 0.67 dB and 0.5 dB, respectively.

V. COMPLEXITY ANALYSIS

Let $M \times N$ be the size of the image to be demosaicked. We first examine the number of computations required by the original ECI method. To estimate a missing green value, Eq. (1) requires 8 additions and 4 bit-shift operations and Eq. (2) needs 4 additions and 1 bit-shift operation, amounting to a total of 12 additions and 5 bit-shift operations. On the other hand, to estimate a missing red or blue value, each of Eq. (3) and Eq. (4) requires 2 additions and 1 bit-shift operation, and Eq. (5) needs 4 additions and 1 bit-shift operation. As there are $MN/2$ missing green values and $3MN/4$ missing red and blue values to be estimated, a total of $12 \times MN/2 + 2 \times (2 + 2 + 4) \times MN/4 = 10MN$ additions and $5 \times MN/2 + 2 \times (1 + 1 + 1) \times MN/4 = 4MN$ bit-shift operations are required by the original ECI method.

For the enhanced ECI method, Eqs. (1), (11), (12) and (13) are used to estimate each missing green value, and they require 31 additions, 8 absolute conversions, 9 multiplications, and 4 bit-shift operations. By using the color difference values obtained from the preceding step, Eqs. (14), (15) and (16) are used to estimate a missing red or blue value, and they require 23 additions, 8 absolute conversions, and 9 multiplications. As for the refinement step, since all the adjacent color different values and their corresponding weights have been obtained in the initial step, only Eqs. (12) and (13) or (16) are required to update an estimated green, red, or blue value, and they need 4 additions and 5 multiplications. All in all, a total of $58MN$ additions, $28MN$ multiplications, $16MN$ absolute conversions, and $2MN$ bit-shift operations are required by the enhanced ECI method.

For the original AP method, the initial interpolation step requires about 10 additions, 4 absolute conversions, and 4 bit-shift operations in Eqs. (6) and (7) to compute each missing green value, and another 5 additions and 3 bit-shift operations to compute three adjacent missing red or blue values, resulting in a total of $7.5MN$ additions, $2MN$ absolute conversions, and $3.5MN$ bit-shift operations for the whole image. As reported in [15], the remaining steps of the original AP method require about $384MN$ additions and $384MN$ multiplications.

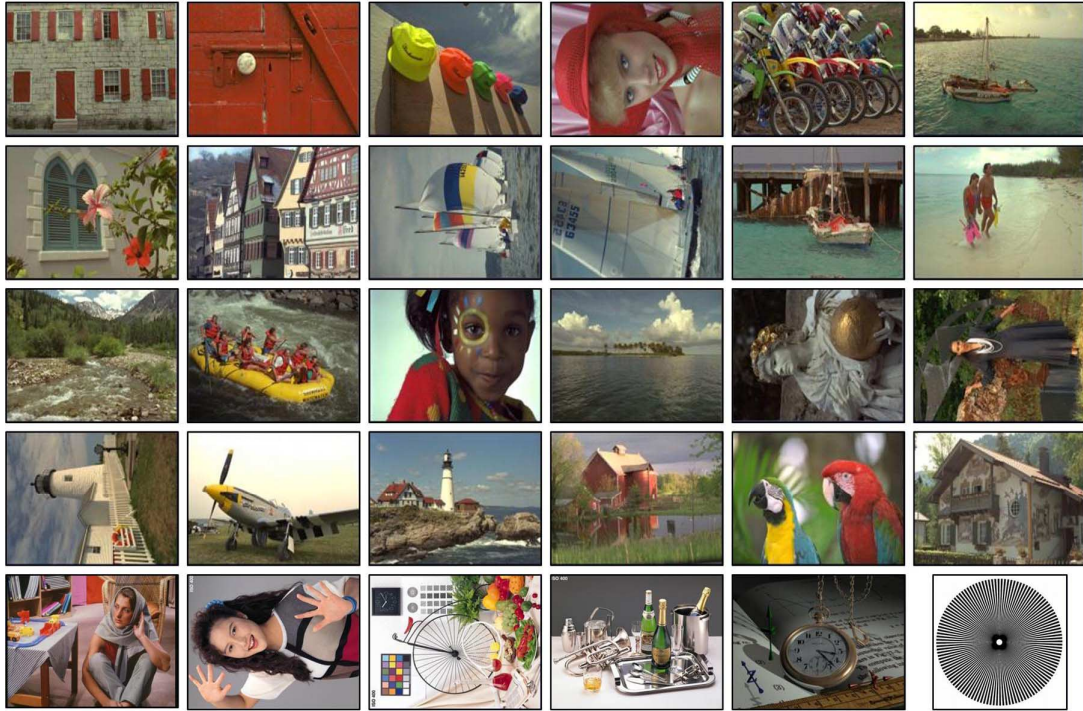


Fig. 6. Test images (referred to as Image 1 to Image 30, enumerated from left-to-right and top-to-bottom.)

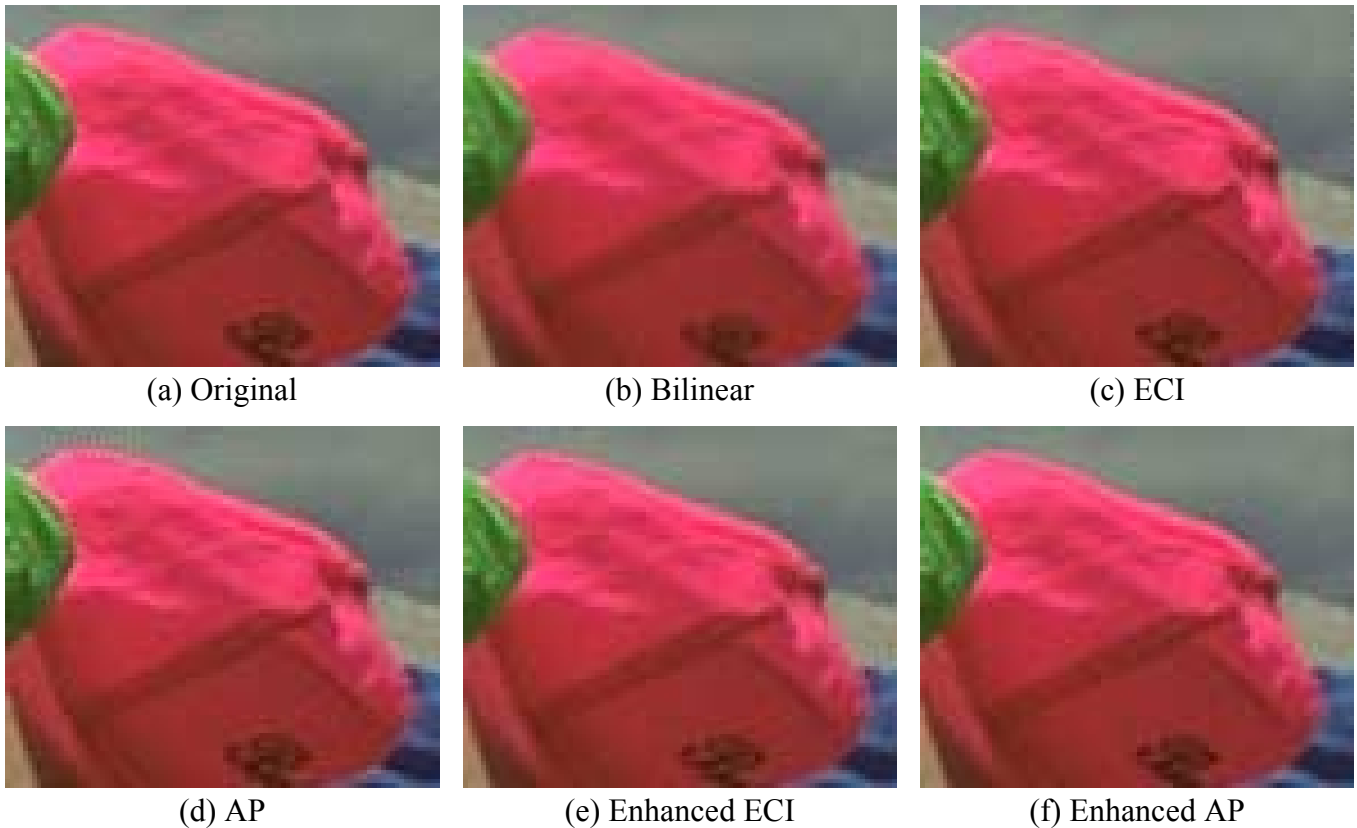


Fig. 7. Cropped region of Cap image: (a) Original, and demosaicked results of (b) bilinear interpolation, (c) ECI method, (d) AP method, (e) enhanced ECI method, and (f) enhanced AP method.

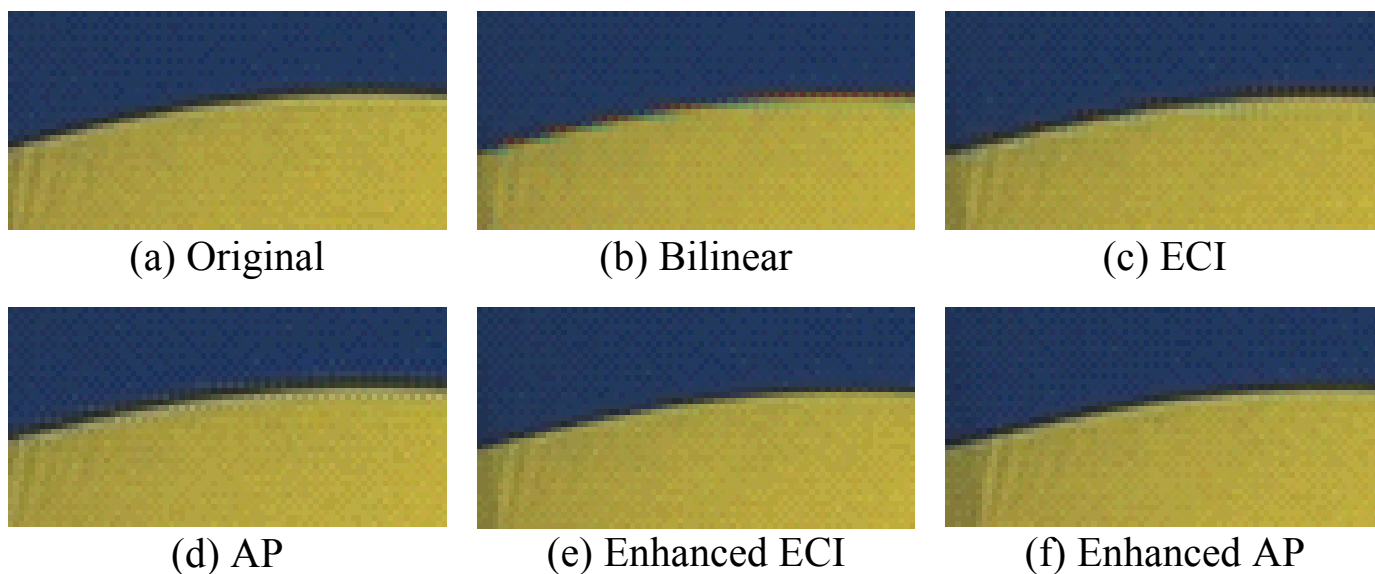


Fig. 8. Cropped region of Sails image: (a) Original, and demosaicked results of (b) bilinear interpolation, (c) ECI method, (d) AP method, (e) enhanced ECI method, and (f) enhanced AP method.

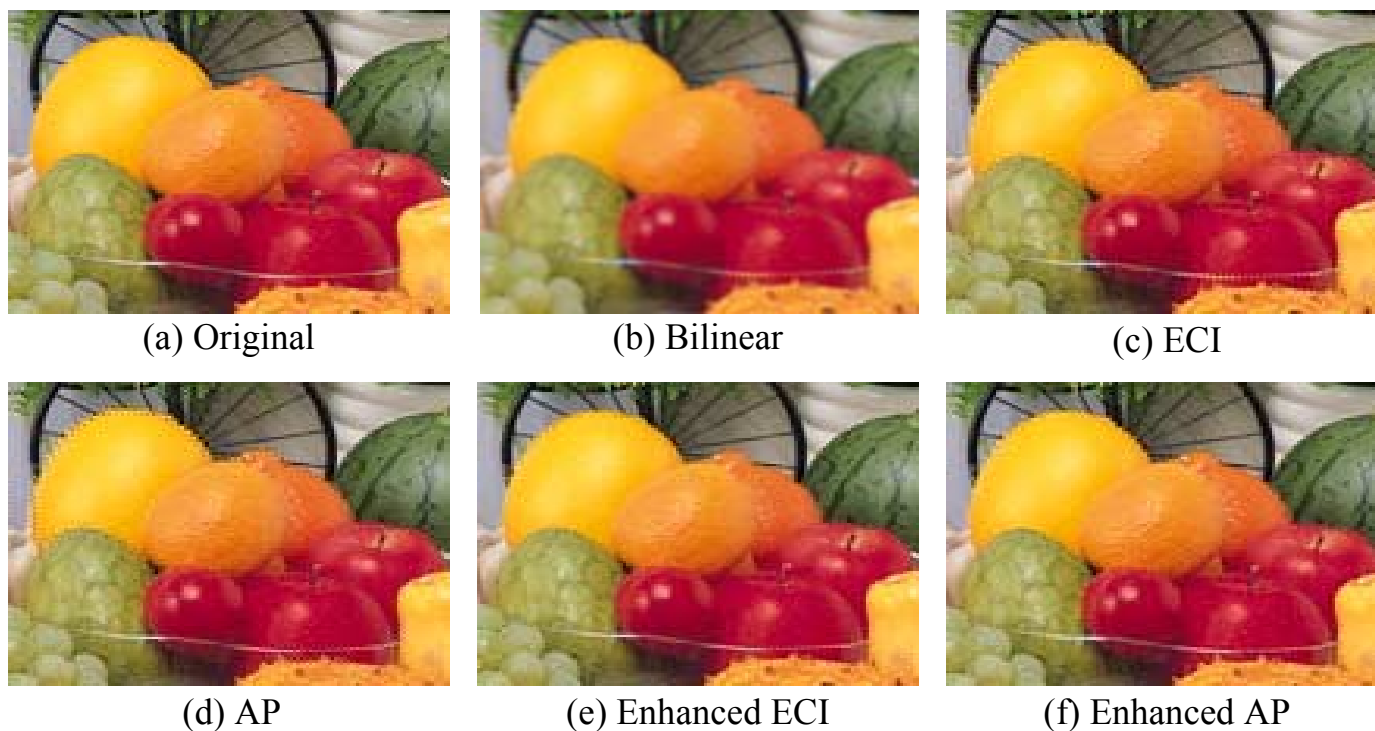


Fig. 9. Cropped region of Bike image: (a) Original, and demosaicked results of (b) bilinear interpolation, (c) ECI method, (d) AP method, (e) enhanced ECI method, and (f) enhanced AP method.

Our modification made to the AP’s initial interpolation requires $50MN$ additions, $16MN$ absolute conversions, $18MN$ multiplications, and $2MN$ bit-shift operations. Additionally, the change made to the green plane updating step takes $76MN$ additions and $55MN$ multiplications. Hence, the

enhanced AP method requires about a total of $510MN$ additions, $16MN$ absolute conversions, $2MN$ bit-shift operations, and $457MN$ multiplications.

TABLE I
DEMOSAICKING PERFORMANCE COMPARISON: PSNR RESULTS (IN dB) OF THE RED, GREEN AND BLUE PLANES ARE LISTED IN
THE 1st, 2nd AND 3rd ROWS FOR EACH IMAGE

Image	Bilinear	Freeman	NEDI	ECI	AP	Enhanced ECI	Enhanced AP	Image	Bilinear	Freeman	NEDI	ECI	AP	Enhanced ECI	Enhanced AP
1	25.31	30.75	33.77	33.21	37.17	37.00	37.86	16	30.30	35.37	39.41	37.51	41.46	40.56	40.93
	29.58	37.08	35.95	35.65	40.02	40.64	40.76		34.73	41.78	41.43	40.14	44.39	44.15	44.17
	35.35	30.90	34.33	33.38	36.96	37.44	37.50		30.39	35.56	39.30	37.32	40.46	40.37	40.02
2	31.89	35.95	37.24	36.85	38.29	38.01	39.62	17	31.63	38.02	36.53	39.14	41.48	41.04	41.87
	36.26	42.36	41.34	41.28	40.20	43.81	41.62		34.54	41.94	39.22	40.35	43.65	43.36	44.01
	32.36	37.77	39.87	39.35	38.73	41.44	40.00		30.86	37.22	36.82	38.59	40.13	40.21	40.33
3	33.45	39.02	39.57	40.51	41.29	41.98	42.42	18	27.32	33.39	33.35	34.92	36.74	36.22	37.03
	37.17	44.27	41.67	43.11	43.23	45.50	44.64		30.54	37.48	36.05	36.54	39.47	39.44	39.60
	33.83	39.08	39.20	40.07	39.82	41.68	41.27		26.82	32.88	34.03	34.82	35.95	36.61	36.22
4	32.61	37.07	36.89	36.88	37.70	37.71	38.90	19	26.78	31.75	36.37	34.53	39.44	38.94	39.63
	36.53	43.44	41.58	42.16	42.15	44.07	43.42		31.74	39.23	38.81	37.23	42.58	42.50	42.71
	32.91	39.44	40.09	40.77	41.29	42.16	42.15		26.95	32.11	37.29	34.76	39.11	39.46	39.02
5	25.75	32.88	31.45	35.04	37.70	37.60	38.92	20	30.81	37.08	37.15	38.93	41.10	41.19	41.80
	29.32	38.82	33.70	36.84	39.42	40.93	40.54		34.58	42.38	39.69	40.56	43.20	44.13	43.76
	25.92	33.02	31.13	34.74	35.53	37.01	36.20		30.59	36.35	36.44	37.48	38.20	39.55	38.60
6	26.7	32.14	35.59	34.65	38.34	37.57	38.21	21	27.63	33.33	34.69	35.63	38.85	38.74	39.38
	31.05	38.56	37.67	36.98	41.21	41.19	41.42		31.54	39.06	37.15	37.57	41.53	41.88	42.04
	27.00	32.30	35.17	34.12	37.07	37.12	36.83		27.53	33.20	34.34	34.97	37.27	37.76	37.48
7	32.57	39.10	38.58	40.31	41.85	42.08	42.66	22	29.84	34.92	35.76	36.41	37.71	37.67	37.95
	36.47	44.18	41.14	42.16	43.32	45.35	44.28		33.34	39.52	38.49	38.64	39.79	40.98	40.35
	32.58	38.84	38.83	39.69	39.54	41.60	40.36		29.22	34.05	35.90	35.74	36.29	37.58	36.69
8	22.53	27.40	30.58	30.16	35.36	34.37	35.60	23	34.43	40.10	40.12	40.84	41.90	41.95	42.97
	27.40	34.87	33.61	33.09	37.99	38.63	38.40		37.98	44.88	42.46	43.84	43.38	45.62	44.36
	22.48	27.40	30.27	29.87	34.26	34.43	34.32		34.12	40.08	40.75	41.68	39.84	42.53	41.02
9	31.56	36.86	39.53	38.66	41.37	41.62	41.89	24	26.40	32.73	30.84	34.37	34.90	34.64	35.41
	35.72	43.09	41.68	41.37	44	44.78	44.26		29.38	36.62	33.74	35.54	37.27	37.60	37.77
	31.38	37.09	40.07	39.32	40.81	41.56	41.11		25.29	30.37	30.13	31.94	32.59	32.99	32.99
10	31.84	38.02	38.14	39.37	41.44	41.28	41.92	25	25.90	30.36	27.04	31.92	32.48	32.51	32.62
	35.37	43.66	40.02	42.07	44.3	45.01	44.77		30.28	36.97	30.23	35.62	36.75	36.97	37.08
	31.23	37.51	38.10	39.43	40.6	41.20	40.94		26.01	30.22	27.10	31.72	32.37	32.33	32.44
11	28.17	33.70	34.98	35.62	38.66	38.24	39.00	26	29.65	34.31	33.76	34.41	35.37	36.45	35.57
	32.22	39.80	37.70	38.06	40.9	42.17	41.41		32.72	38.51	35.99	36.73	39.05	39.60	38.52
	28.34	34.20	35.32	36.09	38.36	39.39	38.53		29.58	34.66	34.22	34.98	36.33	37.10	36.29
12	32.67	37.77	40.17	39.22	42.08	41.76	42.31	27	22.47	28.01	28.59	29.28	30.77	32.37	31.83
	36.82	43.74	42.87	42.40	44.30	45.62	45.00		26.10	33.12	30.48	31.22	33.35	34.85	34.71
	32.35	37.70	40.40	39.38	41.17	41.95	41.36		22.32	27.56	27.97	28.62	30.21	31.43	31.01
13	23.09	29.52	29.52	31.43	34.40	34.24	35.14	28	25.70	31.49	32.42	33.22	35.57	36.53	35.94
	26.49	34.20	32.00	32.64	36.79	36.85	37.66		29.76	37.68	35.34	35.29	38.49	39.78	39.14
	23.00	29.14	29.37	30.64	33.01	33.24	33.52		25.94	31.64	32.65	32.91	34.98	36.18	35.42
14	28.15	33.54	34.41	34.78	35.81	36.10	38.26	29	32.75	38.06	38.22	38.55	39.43	40.99	39.57
	32.01	38.91	37.56	37.87	37.75	40.58	39.86		36.34	43.20	41.39	41.14	42.78	44.72	43.27
	28.60	34.24	34.70	35.15	34.12	36.86	35.78		33.49	39.33	39.10	39.63	40.39	42.63	40.59
15	28.15	35.13	34.76	36.33	38.02	36.97	39.04	30	17.21	23.57	28.25	27.12	32.24	33.38	34.00
	32.01	42.35	39.43	41.11	40.09	42.67	41.47		20.92	30.64	28.00	29.54	35.49	35.90	36.02
	28.60	38.17	37.48	39.31	38.70	40.34	39.58		17.21	23.57	28.17	25.92	32.39	32.95	34.01
Average								28.54	34.04	34.53	35.66	37.96	37.99	38.61	
								32.41	39.75	37.22	38.23	40.56	41.64	41.23	
								28.53	34.19	34.80	35.75	37.22	38.24	37.72	

Table II lists the number of computational operations required by the original and the enhanced ECI and AP methods. According to Table II, the original ECI method is the least complex, followed by the enhanced ECI method, the original AP method, and the enhanced AP method. Although the enhanced ECI method requires more computations than the original ECI method, it is more computationally effective than the original AP method, and performs better, in terms of both visual and PSNR results, than the original ECI and AP methods, as seen in Section IV. The enhanced AP method is the most complex, but compared with the original AP method, the complexity increment is moderate and hence rather acceptable.

VI. CONCLUSION

In this paper, we advocate the importance of exploiting both image spatial and spectral correlations in demosaicking, and characterize the resultant artifacts due to inadequate use of either correlation. Based on the insights gained from our study, we have enhanced two state-of-the-art demosaicking methods, ECI and AP methods, which do not fully utilize the spatial or spectral correlation. We accomplish this by introducing an adaptive-weighted interpolation scheme and/or subband interpolation scheme, making better use of both of the image spatial and spectral correlations. Experimental results suggest that the enhanced methods not only effectively suppress demosaicking artifacts in edge regions, but also obtain better PSNR results when tested with a large variety of popular test images. Furthermore, the computational complexities of the enhanced methods are rather acceptable as compared with the original. In particular, the enhanced ECI method can perform better, both visually and in terms of PSNR values, than the original AP method, and requires much fewer computations.



Lanlan Chang received the B.S. degree in electronics and information engineering from Huazhong University of Science and Technology, P. R. China, in 2003.

She is currently a PhD student with the School of Electrical and Electronic Engineering, Nanyang Technological University, Singapore. Her research interests include image restoration and enhancement.



Yap-Peng Tan (M'97) received the B.S. degree in electrical engineering from National Taiwan University, Taiwan, R.O.C., in 1993, and the M.A. and Ph.D. degrees in electrical engineering from Princeton University, Princeton, New Jersey, in 1995 and 1997, respectively.

He was the recipient of an IBM Graduate Fellowship from IBM T. J. Watson Research Center, Yorktown Heights, New York, from 1995 to 1997. He was with Intel

and at Sharp Labs of America from 1997 to 1999. Since November 1999, he has been a faculty member at the Nanyang Technological University of Singapore. His current research interests include image and video processing, content-based multimedia analysis, computer vision, and pattern recognition. He is the principal inventor on eight U.S. patents in the areas of image and video processing.

TABLE II
COMPLEXITY COMPARISON OF THE ORIGINAL AND THE ENHANCED ECI AND AP METHODS

Method	Number of computational operations			
	Addition	Absolute	Bit-shift	Multiplication
Original ECI	10.0 <i>MN</i>		4.0 <i>MN</i>	
Original AP	391.5 <i>MN</i>	2.0 <i>MN</i>	3.5 <i>MN</i>	384.0 <i>MN</i>
Enhanced ECI	58.0 <i>MN</i>	16.0 <i>MN</i>	2.0 <i>MN</i>	28.0 <i>MN</i>
Enhanced AP	510.0 <i>MN</i>	16.0 <i>MN</i>	2.0 <i>MN</i>	457.0 <i>MN</i>

REFERENCES

- [1] B. Bayer "Color imaging array," U. S. Patent No. 3,971,065, 1976.
- [2] R. Rajeev, E. Wesley, L. Griff, and S. William, "Demosaicking methods for bayer color arrays," *Journal of Electronic Imaging*, 2002.
- [3] J. Adams, K. Parulski, and K. Spaulding, "Color processing in digital cameras," *Proc. of IEEE*, vol. 18, no. 6, pp.20-30, 1998.
- [4] H. Zen, T. Koizumi, H. Yamamoto, and I. Kimura, "A new digital signal processor for progressive scan CCD," *IEEE Trans. Consumer Electronics*, vol. 44, no. 2, pp. 289-296, May 1998.
- [5] J. Adams, "Interactions between color plane interpolation and other image processing functions in electronic photography," *Proc. SPIE Cameras and Systems for Electronic Photography and Scientific Imaging*, vol. 2416, pp. 144-151, 1995.
- [6] T. Kuno, H. Sugiura, and N. Matoba, "New interpolation method using discriminated color correlation for digital still camera," *IEEE Trans. Consumer Electronics*, vol. 45, no. 1, pp. 259-267, Feb, 1999.
- [7] D. Cok, "Signal processing method and apparatus for producing interpolated chrominance values in a sampled color image signal," *U.S. Patent* No. 4,642,678, 1987.
- [8] C. Laroche and M. Prescott, "Apparatus and method for adaptively interpolating a full color image utilizing chrominance gradients," *U.S. Patent* No. 5,373,322, 1994.
- [9] X. Li and M. T. Orchard, "New edge directed interpolation," *IEEE Transactions on Image Processing*, vol. 10, no. 10, 2001.
- [10] S. C. Pei and I. K. Tam, "Effective color interpolation in CCD color filter array using signal correlation," *IEEE Int. Conf. Image Processing*, vol. 3, 2000.
- [11] T. W. Freeman, "Median filter for reconstructing missing color samples," *U.S. Patent* No. 4,724,395, 1998.
- [12] J. Hamilton and J. Adams, "Adaptive color plane interpolation in single sensor color electronic camera," *U.S. Patent* No. 5,629,734, 1997.
- [13] R. Kimmel, "Demosaicking: Image reconstruction from color CCD samples," *IEEE Trans. Image Processing*. Vol.7, no. 3, pp. 1221-1228, 1999.
- [14] B. S. Hur and M. G. Kang, "High definition color interpolation scheme for progressive scan CCD image sensor," *IEEE Transactions on Consumer Electronics*, vol. 47, no. 1, pp. 179-186, Feb. 2001.
- [15] B. K. Gunturk, Y. Altunbasak and R. M. Mersereau, "Color plane interpolation using alternating projections," *IEEE Transactions on Image Processing*, vol.11, no.9, 2002.